MICROPHYSICAL RETRIEVAL FROM DUAL-FREQUENCY GPM OBSERVATIONS

P7.1

Minda Le *, V. Chandrasekar and S. Lim

Colorado State University
1373, campus Delivery
Fort Collins CO 80523-1373, USA

ABSTRACT

Following the success of the Tropical Rainfall Measuring Mission (TRMM), considerable effort has been directed at the next generation of space-based precipitation radar (PR) to be launched aboard the Global Precipitation Measuring (GPM) core satellite. The GPM mission concept is centered on the deployment of a core observatory satellite with an active dual-frequency precipitation radar (DPR), operating at Ku and Ka bands. The DPR aboard the GPM core satellite is expected to improve our knowledge of precipitation processes relative to the single-frequency on microphysics, and better accuracies in rainfall and liquid water content retrievals. This paper presents a new algorithm to retrieve parameters of drop size distribution of GPM-DPR. Models have been built for GPM-DPR classification based on intensive study of APR2 (second generation airborne precipitation radar) data from NAMMA (NASA African Monsoon Multidisciplinary Analysis) experiment.

Index Terms — GPM, DSD (drop size distribution), Classification

1. INTRODUCTION

GPM is a science mission with integrated application goals for advancing the knowledge of the global water/energy cycle variability as well as improving weather, climate and hydrological prediction capabilities through more accurate and frequent precipitation measurements around the global. The GPM mission concept is centered on the deployment of a core observatory satellite with an active dual-frequency (Ku and Ka band) precipitation radar (DPR) which is expected to improve our knowledge of precipitation processes.

* *Corresponding author address:* Minda Le, Colorado State University, Electrical and Computer Engineering Dept. CO. e-mail:leminda@engr.colostate.edu

New algorithms come along with the new DPR to retrieve microphysics of precipitation, such as drop size distribution (DSD) parameters in each resolution volume. Generally, there are two main types of dual-frequency algorithm that can be used within a down-looking space radar. 1) the forward method, where the DSDs are calculated at each bin starting from the top bin and moving down to the bottom; and 2) the backward method, where the algorithm begins at the bottom bin and moves upward to the top. The two types are summarized in Figure1. Forward method has limited application because of a tendency to diverge in regions of moderate-to-heavy attenuation or moderate-to-heavy rainfall (Liao and Meneghini 2004). Backward algorithms can be further divided into three groups: 1) standard dual-wavelength (or DAD); 2) surface-reference technique (SRT); and 3) iterative non-SRT. The basic principle of the standard dual-wavelength approach is to estimate the path attenuation and rain rate using the radar equation and the ratio of the returned power of both wavelengths. This method requires one of two assumptions: first, the rain rate must be uniform over the measurement interval; or second, the reflectivity factor must be wavelength independent, meaning Rayleigh scattering at both frequencies (Iguchi et al, 2005). The SRT method uses a backward calculation method which is more stable than forward method but requires a priori knowledge of the total two-way path-integrated attenuation (PIA) for each ray or an ability to calculate it (Meneghini et al. 1997, 2002). The third method, the non-SRT algorithm, is a self-consistent algorithm wherein the total PIA for each frequency channel is first estimated using initial guess then optimized it through an iteration process (see Mardiana et al. 2004). However, both forward and backward methods mentioned above suffer from multi-valued solution when retrieving median volume diameter D_0 for rain described in detail by Liao et al.(2003), Mardiana et al (2004), and Meneghini et al.(2002). Rose and Chandrasekar (2006) proposed a supplementary method, using linear assumption of

vertical profiles for D_0 and N_w (in log scale) in rain region to avoid the bi-valued problem.

In this paper, a hybrid approach combing the advantages of forward method and recursive backward method is proposed and evaluated. Forward method is applied to ice and melting ice region to avoid large attenuation while linear assumption is applied in rain region. No SRT information is needed in this algorithm. The proposed algorithm uses an iteration procedure to optimize DSD parameters at the bottom of rain region by constructing the cost function along the whole vertical profile. The performance of the algorithm is tested using simulated DPR observations from NAMMA experiment data.

The proposed DSD retrieval algorithm relies on a classification method for the DPR observations including two models. 1) the model to classify stratiform , convective or other type vertical profile ; 2) the model to detect the melting layer region for stratiform and convective vertical profile respectively. The two classification models are built based on an intensive study of the NAMMA experiment data in 2006.

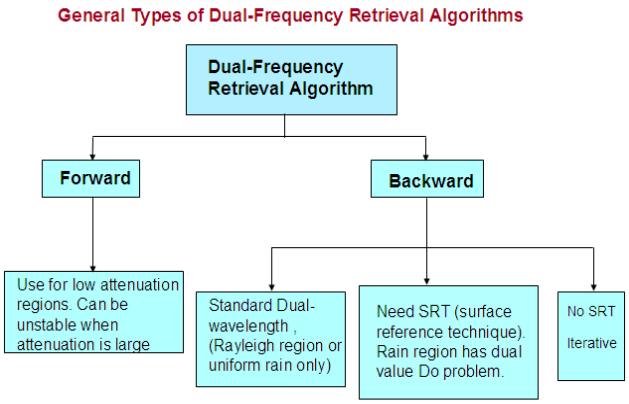

Figure 1, General types of dual-frequency retrieval algorithm.

2, GPM-DPR CLASSIFICATION MODELS

APR2 data during NAMMA experiment in 2006 is used and studied to build the models which might be useful in GPM-DPR precipitation classification.

DPR offers dual-frequency observations which will provide us a new way to investigate the microphysical properties using the difference between two frequency observations (DFR). There are two main reasons that will cause the difference between two frequency channels: one is the non-Rayleigh scattering effect; another is path attenuation. Within the ice and melting ice region, DFR is mainly caused by non-Rayleigh scattering effect while starting from the rain region, the path attenuation difference will be the main reason that cause DFR to increase sharply. When converting from ice to melting ice region, the change in dielectric constant due to the melting of hydrometer particles will have different effect on Ku and Ka band discussed by Bringi and Chandrasekar, (2001), thus provide us a signature to detect this transition by DFR. In a word, DFR might be an ideal parameter to detect hydrometer transition from ice to melting ice and to rain region. Meanwhile, for stratiform and convective rain type, our study will show the difference on their DFR vertical profiles respectively.

2.1 Model 1: to classify stratiform, convective and other type rain

Self organized map (SOM) method is used to classify good NAMMA data based on vertical profiles. Stratiform and convective rain types show their typical vertical profile of DFR in Figure 2.

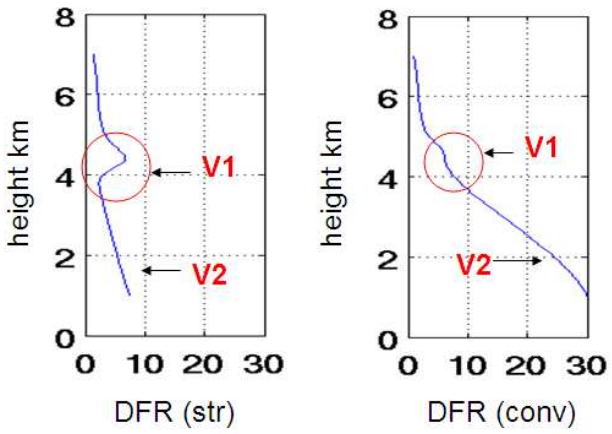

Figure 2, Typical vertical profile of DFR (dual-frequency ratio) for stratiform rain (left) and convective rain (right).

The left subplot shows the typical vertical profile of DFR for stratiform rain type with a clear hydrometer phase transition corresponding to a bright band region. Meanwhile, although DFR has a sharp increase in rain region, its magnitude toward surface won't exceed around 10-15 dBZ, indicating the attenuation in rain is not very strong. For convective rain type, which in shown in the right subplot, the transition from ice to melting ice is not as clear as stratiform rain, and the magnitude of DFR toward surface will normally exceed around 20 dBZ. In order to enlarge the contrast

between stratiform and convective rain type and make the classification criteria more simple and applicable, in this study, ratio between V1 and V2 (as can be seen from Figure 2) is used to do classification of model 1.

V1 here is the difference between local maximum and minimum of the DFR profile as seen by red circle in Figure 2. V2 is defined as mean value of DFR profile between 1.5 to 2.5 km, in case to avoid surface clutter effect and not weaken the contrast. As we can see, for stratiform rain, V1 is easy to be detected and with relative larger value than convective case. Also, V2 in stratiform rain is usually smaller than convective case which makes the ratio (=V1/V2) a better parameter to be used in classification than either V1 or V2.

To decide the threshold of ratio for model 1, some statistical studies are done to calculate CDF (cumulative density function) of ratio based on a certain rain type decided by SOM result. As can be seen from Figure 3, 95% confidence line gives DFR ratio smaller than 0.17 for SOM based convective profiles. While for stratiform case, this value is 0.35

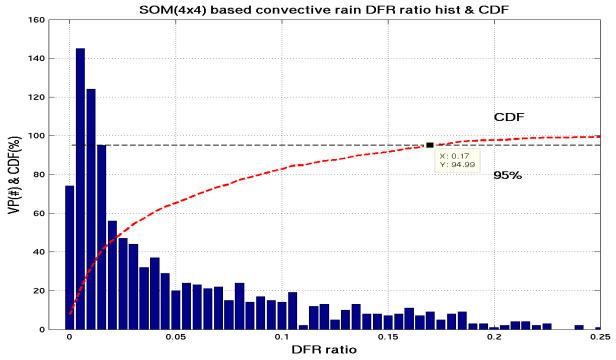

Figure 3, Histogram of DFR ratio of SOM based convective profiles and the CDF.

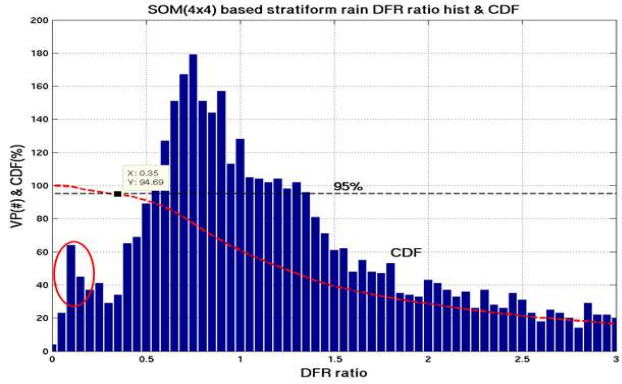

Figure 4, Histogram of DFR ratio for SOM based stratiform profiles and the CDF.

(larger than) as shown in Figure 4. Since there are still some vertical profiles (around 2% of SOM based stratiform profiles) show DFR ratio smaller than 0.17 which are circled in figure 4. This confusion can be solved by adding another constraint using typical V2 values for stratiform and convective case. Same plots as figure 3 and 4 are made based on V2 value, and 95% confidence line hits 10 dBZ and 17 dBZ respectively for stratiform and convective case.

Therefore, based on the statistics study of all good NAMMA experiment data, the criteria and thresholds for classification model 1 is summarized as follows: Stratiform: ratio >=0.35 and V2 <=10; Convective : ratio<=0.17 and V2>=17; The rest profiles are classified as other type. This model 1 is applied to one overpass of NAMMA data with both stratiform and convective case in it as shown in Figure 5. A, B and C labels represent the stratiform, convective and other type profile classified by model 1. The vertical profile of A, B and C are shown in Figure 6, 7, 8 respectively. The DFR profiles in Figure 6, 7, 8 satisfy the criteria used in model 1 and correctly display the typical signature of the types.

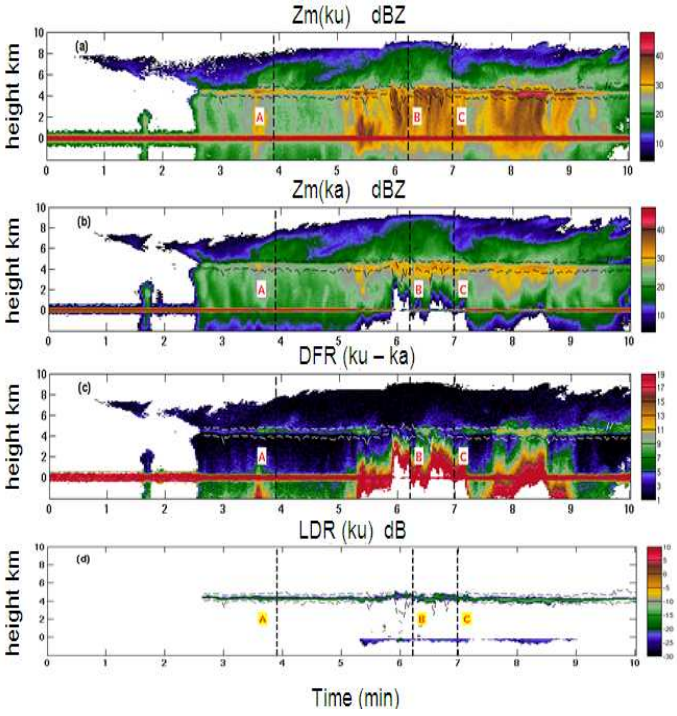

Figure 5, Overpass of NAMMA experiment 20060903-142134 case. From top row to bottom row are Zm(Ku), Zm(Ka), DFR,LDR(Ku). A, B, C label indicates stratiform, convective, other type respectively by classification model 1. Dashed lines in each subplot indicates melting layer region detected by classification model 2.

2.2 Model 2: to detect melting layer region

As discussed in section 2, DFR is an ideal parameter to detect the hydrometer phase transition. Therefore, the main parameter used in model 2 is DFR and its slope. For stratiform case (label A) as shown in Figure 6, DFR has very clear trend of starting to increase at the melting layer top, hitting the local maximum, then starting to decrease at bottom half of the bright band, and finally, increasing sharply indicating attenuation in rain. The dashed line in Figure 6 is the melting region decided by DFR and its slope. Melting layer top height is decided by the local maximum position of the DFR slope, since it will correspond to the sharpest increase of DFR from ice to melting ice transition. Melting layer bottom height is detected by local minimum of DFR profile, which is a quite clear feature that rain region starts.

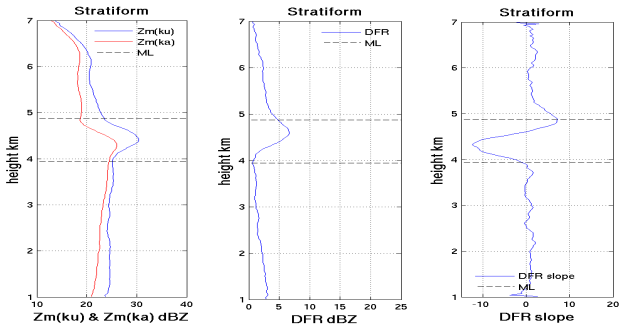

Figure 6, Stratiform profile (label A) from Figure 5, and its DFR and DFR slope profile.

For convective profile (label B), melting layer detection is more complicated since for some cases, melting layer region is not obvious. As shown in Figure 7, melting region might not be easily detected by the same method used as for stratiform case. In stead, we use the slope of $Z_m(ku)$ to detect melting layer top. The local maximum of $Z_m(ku)$ slope corresponds to the sharpest increase of reflectivity profile which is also a signature to enter the melting region. The parameter used to detect melting layer bottom is DFR slope. The transition from melting region to rain for convective case, though not very obvious in DFR, could be detected by its slope. A trend in DFR slope from local minimum to local maximum corresponds to the transition from melting layer to rain region. Therefore, the mean value of the heights consistent with local minimum and maximum of DFR slope is calculated and regarded as the melting layer bottom in model 2.

The melting layer could also be detected for other type profile classified in model 1, as shown in Figure 8. For this other type, DFR and its slope is more detectable than convective case, so the method used for stratiform case could also be used for other type case.

The dashed line in Figure 5 is the detected melting layer region for one overpass of NAMMA data using model 2. The last row of Figure 5 is the overpass plot of LDR parameter which is regarded as an indication of the melting layer region (Bringi and Chandrasekar, 2001). The model 2 result shows good agreement compared to LDR parameter with a little more wider melting width. This small difference might be caused by the hard threshold of -26 dB for LDR which might be different taking into account different hydrometer type. Furthermore, the melting layer top detected from different methods could correspond to different melting states.

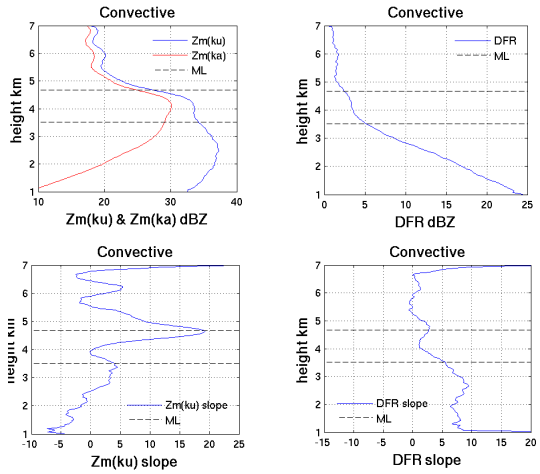

Figure 7, Convective profile (label B) from Figure 5, and its DFR, Zm(ku) slope and DFR slope profile.

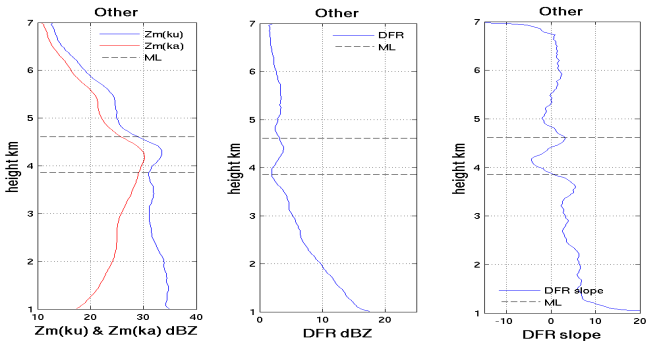

Figure 8, Other type profile (label C) from Figure 5, and its DFR and DFR slope profile.

3, ALGORITHM USED TO RETRIEVE DSD FROM GPM-DPR OBSERVATIONS

The dual-wavelength integral equations described by Meneghini et al. (1997) solve for D_0 and N_0 at each range gate based on the assumed microphysical models for regions are often used in space radar with D_0 retrieved from DFR. But it suffered from multi-valued D_0 problem for rain region. This section redevelops similar integral equations in terms of normalized intercept parameter N_w instead of N_0 and combine forward method which is normally used for ice and melting ice region in space radar and the linear assumption for rain profile (Rose and Chandrasekar, 2006). The proposed hybrid algorithm will be applied for the complete vertical profile including ice, melting ice and rain region in an iterative process without a prior knowledge of SRT. The performance of the algorithm will be tested using simulated Ku and Ka band profiles from NAMMA experiment data.

3.1 Background

Natural variation of drop size distribution can be parameterized adequately by Gamma model (Ulbrich, 1983). This model can be expressed in normalized form as (Bringi and Chandrasekar, 2001).

$$N(D) = N_w f(\mu)\left(\frac{D}{D_0}\right)^{\mu} e^{-\Lambda D} \quad (1)$$

where

$$\Lambda = \frac{3.67 + \mu}{D_0} \quad (2)$$

$$f(\mu) = \frac{6}{3.67^4}\frac{(3.67+\mu)^{\mu+4}}{\Gamma(\mu+4)} \quad (3)$$

where Γ is the gamma function, D_0 is the median volume diameter (mm), μ is the shape factor and N_w ($mm^{-1}m^{-3}$) is the normalized intercept parameter of gamma distribution. In the new algorithm, μ is regarded as fixed number. μ=0 is used for ice and melting ice region while μ=3 is used for rain.

3.2 Algorithm Description

The proposed algorithm can be described as follows. First, calculate estimated DSD using the hybrid method. Second, reconstruct Z_m (refer to estimated $\tilde{Z}_m$) based on estimated DSD and assumed scattering model. Third, test the cost function generated using

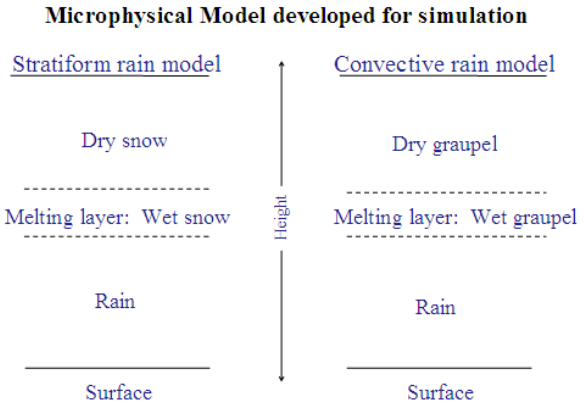

Figure 9, Microphysical model developed for simulation.

reconstructed and observed reflectivity measurements till it converges. The state vectors for this iterative process are D_0 and $\log(N_w)$ of surface. The scattering model used in the retrieval algorithm is listed in Figure 9.

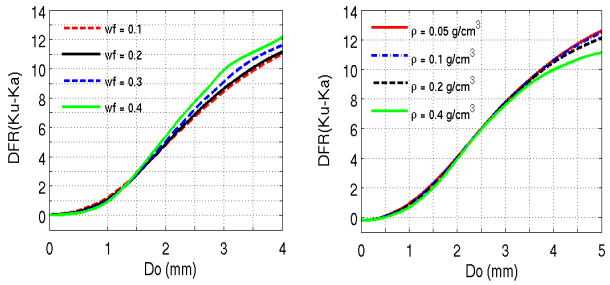

Figure 10, Left: DFR versus D_0 for melting ice with water fraction of 0.1, 0.2, 0.3, 0.4; Right: DFR versus D_0 for ice with snow densities of 0.05, 0.1, 0.2, 0.3 g/cm^3 ;

Following commonly practiced notations in the literature (Bringi and Chandrasekar, (2001), Meneghini et al.(1992)), the governing equations of this hybrid algorithm can be written as follows. Let $\tilde{Z}_{mi}(r)$ be the estimated measured reflectivity. A tilde (~) indicates it is algorithm derived value. The subscript $i(i=1,2)$ represents the particular frequency (13.6 and 35.6 GHz, respectively). Z_{ei} is intrinsic reflectivity while A_i is two-way path integrated attenuation . The measured reflectivity can be written in term of the intrinsic values and attenuation as

$$\tilde{Z}_{mi}(r) = \tilde{Z}_{ei}(r)\,\tilde{A}_i(r) \quad (4)$$

Where the intrinsic reflectivity can be related to the DSD parameters as

$$\tilde{Z}_{ei}(r) = \tilde{N}_w(r) f(\mu) \tilde{D}_0^{-\mu} I_{bi}(\tilde{D}_0), \quad (5)$$

$$\tilde{A}_i(r) = \exp[-0.2\ln(10)h\sum_{n=1}^{j}\tilde{\alpha}_i(r_n)], \quad (6)$$

I_{bi} is a function of $\tilde{D}_0$ which can be expressed as

$$I_{bi}(\tilde{D}_0) = C_{zi}\int_D \sigma_{bi}(D)D^{\mu}e^{-\Lambda D}dD, \quad (7)$$

$$C_{zi} = \frac{\lambda_i^4}{\pi^5|K_w|^2}, \quad (8)$$

σ_b is the backward scattered cross section and λ represents wavelength. K_w is defined as

$$K_w = \frac{m^2-1}{m^2+1}, \quad (9)$$

where m is the complex index of refraction of water. The specific attenuation $\tilde{\alpha}_i$ in (8) is defined as

$$\tilde{\alpha}_i(r) = \tilde{N}_w f(\mu)\tilde{D}_0^{-\mu} I_{ti}(\tilde{D}_0) \quad (10)$$

where

$$I_{ti}(\tilde{D}_0) = C_{ki}\int_D \sigma_{ti}(D)D^{\mu}e^{-\Lambda D}dD, \quad (11)$$

$$C_{ki} = 4.343\times10^{-3}. \quad (12)$$

The estimated $\tilde{D}_0$ and $\tilde{N}_w$ used in (5) are derived using hybrid method described in (13)-(15) for ice as well as melting ice region and (16)-(17) for rain region.

$$DFR(r) = (Z_{m1}(r)+A_1(r)) - (Z_{m2}(r)+A_2(r)), \quad (13)$$

$$\tilde{D}_0(r) = F^{-1}(DFR(r)), \quad (14)$$

$$\tilde{N}_w(r) = \frac{Z_{mi}(r)}{f(u)\tilde{D}_0^{-u}(r)I_{bi}(\tilde{D}_0(r))A_i} \quad (15)$$

$$\tilde{D}_0(r_j) = \frac{D_0(mlb)-D_0(surf)}{length(rain\_region)} * num\_bin + D_0(mlb); \quad (16)$$

$$\tilde{N}_w(r_j) = 10^{\frac{\log N_w(mlb)-\log N_w(surf)}{length(rain\_region)} * num\_bin + \log Nw(mlb)]}; \quad (17)$$

A_i is calculated using similar equations as (6). “mlb” and “surf” in (16) and (17) represent melting layer bottom and surface respectively. The relationship between DFR and D_0 for the ice and melting ice is plotted in Figure 10. The residual of the difference between retrieval and observation is expressed as

$$CF = \sum_{j=1}^{r_N}[\tilde{Z}_{m1}(r_j) - Z_{m1}(r_j)]^2 + [\tilde{Z}_{m2}(r_j) - Z_{m2}(r_j)]^2 \quad (18)$$

The proposed algorithm calculates N_w and D_0 at each resolution volume using the initial guess of $D_0(surf)$ and $\log N_w(surf)$ which will be adjusted till the cost function is minimized. The diagram of the proposed algorithm is shown in Figure 11.

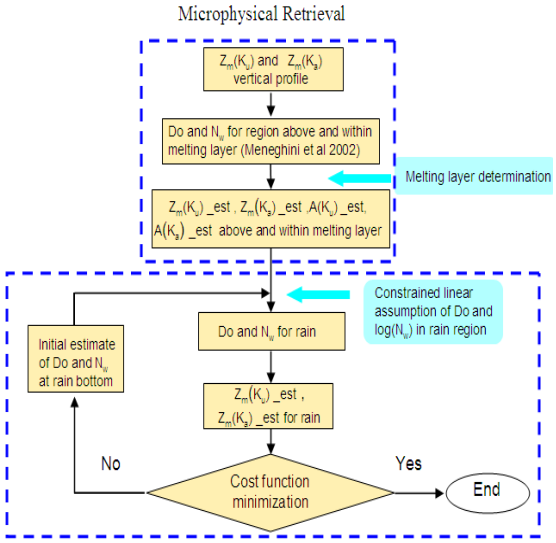

Figure 11, Diagram of DSD retrieval algorithm for GPM-DPR

3.3 Evaluation with simulated vertical profiles

The performance of the algorithm is evaluated using profiles simulated from NAMMA data at label A and B in Figure 5. The simulation process involves three steps: 1) Retrieve DSD from NAMMA data; 2) re-map retrieved DSD to GPM resolution; 3) simulate to Ku and Ka band observations based on the re-mapped DSD.

The output of step 3) will go through the new DSD retrieval algorithm and get the optimized DSD which can be compared with the output of step 2), the simulation truth. The method used in step 1) is another DSD retrieval algorithm using combination of forward method and DAD (difference of attenuation difference) described in Iguchi, (2005). The melting layer region detected in model 2 in section 2 will be used as the boundary information for simulation.

Figure 12 shows the simulated profiles and these profiles will be used to test the new DSD retrieval algorithm, the results of which are shown in Figure 13 by using the same model in simulation as in retrieval. DFR profiles in Figure 12 also show the typical signature of ice, melting ice and rain region as discussed in detail in section 2.The initial guess of D_0 and $\log(N_w)$ at surface is [3, 3] in the algorithm test.

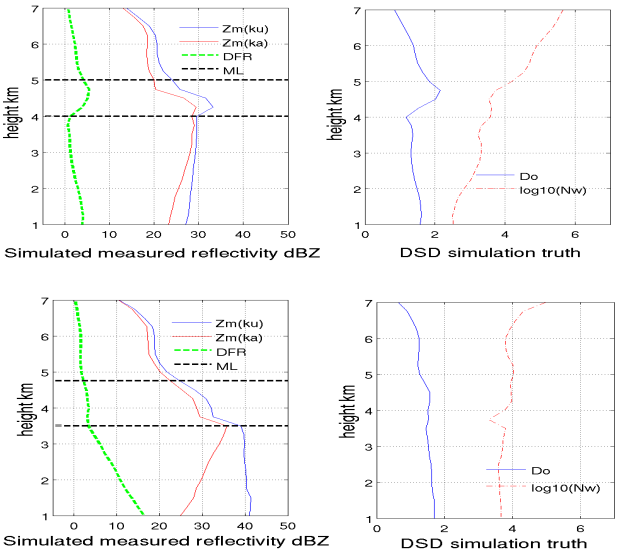

Figure 12, Vertical profile simulated from NAMMA data. Top row: stratiform profile (from label A) and its true DSD in simulation; Bottom row: convective profile (from label B) and its true DSD in simulation.

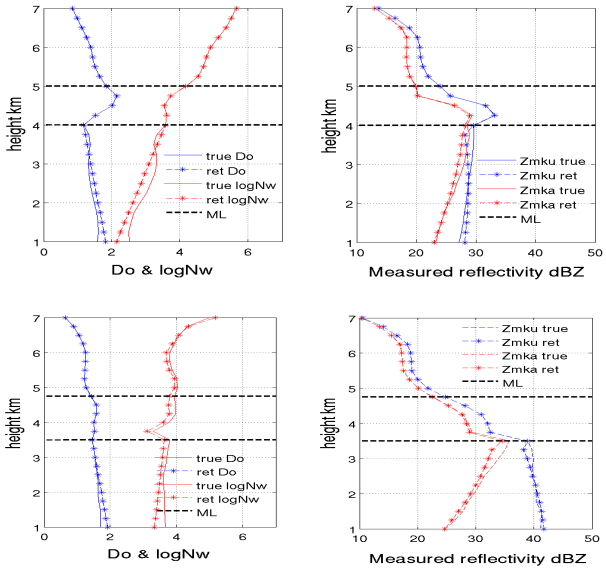

Figure 13, Top left: comparison between retrieved DSD and simulation truth for stratiform profile; Top right: comparison between estimated reflectivity measurements and the simulation truth; Bottom row: the same comparison for convective profile.

In Figure 13, both stratiform and convective profiles show good agreement between simulation truth and algorithm retrieved values. The difference in rain region is caused by the deviation from the actual data to the linear assumption.

The sensitivity of snow density to the algorithm is also tested for both stratiform and convective profile. In simulation, the density of snow particle is 0.1 g/cm^3 and 0.4 g/cm^3 for stratiform and convective profile respectively. While in retrieval, density of 0.2 g/cm^3 and 0.3 g/cm^3 is used. The performance of the sensitivity test is shown in Figure 14. Both subplots show D_0 is not sensitive to the snow density change while $\log(N_w)$ is more sensitive. It shows around 12% underestimate of $\log(N_w)$ in frozen region for the stratiform profile.

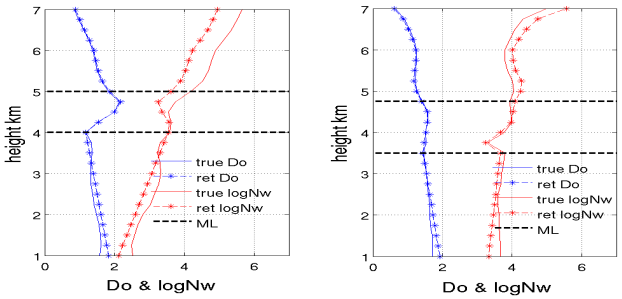

Figure 14, Sensitivity test of snow density change to the DSD retrieval algorithm for stratiform (left) and convective (right) profile. In simulation, snow density of 0.1 g/cm^3 and 0.4 g/cm^3 are used while snow density of 0.2 g/cm^3 and 0.3 g/cm^3 is used in retrieval.

System bias and noise are added to the simulated reflectivity profile to test their effects on the algorithm. First two rows of Figure 15 show the bias sensitivity by applying different bias types on reflectivity profile for stratiform case only for brevity. From the top row of the figure, D_0 is not affected much from the system bias since the bias for both reflectivity channels are the same while $\log N_w$ is affected by the system bias. The reason is that D_0 is retrieved by DFR, where bias from two channels cancels out, but $\log N_w$ is retrieved using both retrieved D_0 and the reflectivity measurements. The second row of Figure 15 shows the algorithm is affected by system bias if the bias of two reflectivity

channels is different. The bottom row of Figure 15 shows the noise test. Random signal fluctuation is generated that reflectivity measurement errors at both channels correspond to 1 dBZ.

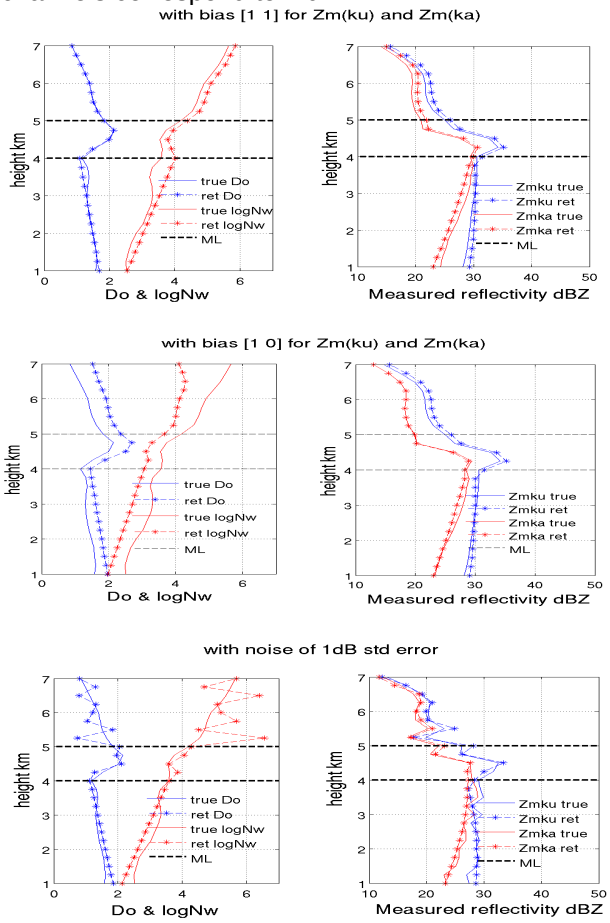

Figure 15, System error test for stratiform profile. Top row: algorithm test with system bias [1 1], which represents 1 dBZ bias for both Zm(Ku) and Zm(Ka) measurements; Second row: algorithm test with system bias [1 0], which represents 1 dBZ and 0 dBZ bias for Zm(Ku) and Zm(Ka) measurements respectively. Bottom row: algorithm test with system noise only.

4. SUMMARY

This paper describes a hybrid DSD retrieval algorithm for GPM-DPR. This algorithm is based on combining the forward method and backward iterative method. An advantage of this algorithm is to avoid multi-valued median drop diameter, a problem for rain faced by dual frequency systems. Also, the proposed algorithm doesn't need a prior knowledge of SRT which is not accurate or even not available sometimes.

Classification models are built from NAMMA data including a stratiform, convective type classification model and a melting layer detection model. The classification model is applied to a NAMMA overpass and compared with LDR data. Good agreement shows this classification model might be useful in GPM-DPR classification where no LDR data is available.

The performance of the algorithm is tested using simulated profiles from NAMMA experiment data. Comparison between algorithm retrieved DSD and simulation truth shows good agreement. The sensitivity of snow density is also tested showing that the retrieval of N_w in log scale will be more sensitive to snow density change than D_0 does. The limitation of this algorithm lies in two aspects: the linear assumption for the rain region and the accuracy of retrieval at melting layer bottom. The algorithm tested with system error will be studied intensively for the next step.

ACKNOWLEDGEMENT

This research is supported by the NASA GPM/PMM program.

REFERENCES

Bringi, V. N., and V. Chandrasekar, 2001: *Polarimetric Doppler Weather Radar -Principles and Applications.* Cambridge University Press.

Iguchi, T, 2005:Possible algorithm for the dual-polarization precipitation radar (DPR) on the GPM core satellite. *32nd Conf. on Radar Meteorology, Amer. Meteor. Soc.,* Albuquerque, NM, CD-ROM.

Liao, L., R. Meneghini, T. Iguchi, and A. Detwiler, 2003: Validation of snow parameters as derived from dual-wavelength airborne radar. Preprints, *31th Int. Conf. on Radar Meteorology,* Seattle, WA, Amer. Meteor. Soc., CD-ROM, P3A.4.

Liao, L., and R. Meneghini, 2004: On study of air/space-borne dual-wavelength radar for estimates of rain profiles. *Third Int. Ocean-Atmosphere Conf.*, Beijing, China, Institute of Atmospheric Physics of Academic Sinica, CD-ROM.

Mardiana, R., T. Iguchi and N. Takahashi, 2004: A dual-frequency rain profiling method without the use of a surface reference technique. *IEEE Trans. Geosci. Remote Sens*., 42, 2214-2225

Meneghini, R, H. Kumagai, J. R. Wang, T. Iguchi and T. Kozu, 1997: Microphysical retrievals over stratiform rain using measurements from an airborne dual-wavelength radar radiometer*. IEEE Trans. Geosci. Remote Sens.,* 35, 487-506.

Meneghini, R, L. Liao and T. Iguchi, 2002: Integral equations for a dual-wavelength radar. *Proc. Geoscience and Remote Sensing Symp., IGARSS'02*, Toronto, ON, Canada, IEEE, 272-274.

Rose, C. R. and V. Chandrasekar, 2005: A system approach to GPM dual-frequency retrieval. *IEEE Trans. Geosci. Remote Sens*., 43, 1816-1826.

Rose, C. R. and V. Chandrasekar, 2006: A GPM dual-frequency retrieval algorithm: DSD profile optimization method. *J. Atmos. Oceanic Technol*, 23, 1372-1383.

Ulbrich, C.W. 1983: Natural variation in the analytical form of the raindrop-size distribution. *J.Climate Appl. Meteor*., 22, 1764-1775.